Journal of Radioanalytical and Nuclear Chemistry
https://doi.org/10.1007/s10967-022-08415-w

# Simulation study of stopping power and damage profiles of H/He plasma irradiation in tungsten and its alloys for fusion power plant

**Meriem El Marsi**[1] · **Zakaria Elmaddahi**[1] · **Imad Fechtal**[1] · **Aouatif Dezairi**[1]

Received: 3 April 2022 / Accepted: 21 June 2022


**Abstract**
Tungsten (W) plays a crucial role in the lifetime of the plasma-facing components of DEMO. In order to avoid oxidation, W-based alloys have been studied as alternatives to W. In this work, the Monte Carlo SRIM-2013 simulation program was used to calculate the nuclear stopping power, electronic stopping power, amount of target vacancies, displacements, replacement collisions, and total target damage of W, W-Cr-Si, W-Cr-Ti, and W-Cr-Y by hydrogen and helium ion bombardment. It is found that W is resistant to vacancies, atomic displacement, and total damage compared to W-based alloys.

**Keywords** Tungsten · Smart alloys · Plasma irradiation · Monte Carlo simulation · Stopping power · Collision events

## Introduction

The European Union Demonstration Fusion Power Plant (EU-DEMO) will be the first power plant based on nuclear fusion reactions able to produce net energy to be delivered to the European electrical grid around 2050 [1]. This device is the next step after the International Thermonuclear Experimental Reactor (ITER) with the final objective of a commercial fusion power plant; the confinement needs to maintain the plasma in place while preserving its density even at higher temperatures than in ITER [2, 3]. The important role of the plasma-facing components (PFCs) for the first wall of future tokamaks is to be compatible with the requirements of plasma purity and to provide adequate protection of in-vessel structures and sufficient heat exhaust capability [4]. Tungsten (W) is deemed as a promising plasma-facing material for the future DEMO reactor because it withstands extreme particle, heat, and radiation loads without forming long-lived radioactive waste. Among the advantages of W for fusion applications are: low sputtering yield by plasma ions, excellent thermal conductivity, low neutron activation, good sputtering threshold energy, and low retention of radioactive tritium. In addition, it has the highest melting temperature of any available metal (3680 K) [5]. In burning plasma conditions, tungsten suffers irradiation of helium (He) in addition to that of hydrogen (deuterium and tritium) fuel [6]. However, the use of W poses a significant safety problem in case of a loss-of-coolant accident (LOCA) with simultaneous air ingress into the reactor vessel. In order to keep the W advantageous features and to counteract its undesirable oxidation, the new advanced so-called ‘‘smart alloys’’ have attracted extensive attention [7]. Self-passivating smart tungsten alloys were originally proposed and developed by Koch and bolt [8]. Alloying elements in the bulk form a dense oxide scale protecting the underlying W alloy from fast oxidation and sublimation of $WO_3$ [9–11]. The first studies of smart alloy systems have been started from experiments with tungsten binary and later tungsten ternary film alloys [12, 13]. Recently, researchers have turned their attention to the W ternary alloy. They first considered adding passivation elements: silicon (Si), titanium (Ti), and yttrium (Y) to the binary W-Cr system in order to observe their antioxidation properties and to improve the performance of the matrix materials [14, 15]. In tokamak devices, plasma-surface interaction (PSI) causes serious surface damage like vacancies, atomic displacement, nuclear stopping power, sputtering, etc. These processes are strongly dependent on the type of both projectile ion and target material. Therefore, PSI leads to a lifetime limitation of materials and degradation of plasma performance

✉ Meriem El Marsi
elmarsimeriem@gmail.com

[1] Condensed Matter Physics Laboratory, Faculty of Science Ben M’sik, Hassan II University of Casablanca, Av. D. El Harty,
B.P 7955, 20663 Casablanca, Morocco

due to contamination by the released impurities [16, 17]. An important quantity used to predict and understand the effects of particle radiation in the matter and the damage produced by energetic particles in diverse contexts, is stopping power [18]. It is a measure of the ability of a material target to slow down energetic particles that travel in its interior. Andersen et al. [19] concluded that for metal targets where the nuclear stopping power determines the sputtering yield. There are various semi empirical and theoretical models providing stopping power estimates for different combinations of ions and materials. We can mention here, for instance, Meluzova et al. [20] calculated the electronic stopping power for the hydrogen atoms in tungsten, carbon and beryllium targets. Zinov et al. [21] studied the nuclear stopping power of hydrogen and helium isotopes in beryllium, carbon, and tungsten.

The computer code, Stopping and Range of Ions in Matter or SRIM is an extremely popular used as a reference in the radiation effects research to predict damage production. This software uses modern theoretical models and experimental databases. It is based on the binary collision approximation (BCA) model with the Monte Carlo (MC) method using a quantum mechanical treatment of ion-atom collisions [22].

In this work, we aim to study the behavior of nuclear stopping power, electronic stopping power, the total number of vacancies, the total number of displacements, the number of replacement collisions per angstrom per ion, and total target damage of W, W-Cr-Si, W-Cr-Ti, and W-Cr-Y as a function of primary $H^+$ and $He^+$ bombarding energy by using SRIM-2013 software. Furthermore, the comparison between these materials for the plasma-facing components is elucidated in this paper.

## Theory

The total stopping power of the material is defined as the mean energy loss per unit length suffered by charged particles traversing material due to Coulomb interactions with atomic nuclei and the electrons of the material. It is described by equation [23]:

$$S(E) = -\frac{dE}{dx} = S_e(E) + S_n(E) \tag{1}$$

Where the stopping powers with subscript n and e represent nuclear and electronic stopping power respectively. The most commonly encountered unit is [eV/$10^{15}$/cm$^2$].

The SRIM program is based on Ziegler et al. approach (1985) [24]. The nuclear stopping cross section $S_n(E)$ of the fitting formula given by Ziegler et al. can be depicted as [25]:

$$S_n(E) = \frac{8.462 Z_1 Z_2 S_n(\varepsilon)}{\left(1+M_2/M_1\right)\left(Z_1^{0.23}+Z_2^{0.23}\right)} \left[10^{-15} eV.cm^2\right] \tag{2}$$

Where $Z_1$ and $Z_2$ are the atomic numbers for each of the incident ion and material target respectively, and $S_n(\varepsilon)$ is the reduction of nuclear cross section.

Ziegler et al. [26] compiled the existing electronic stopping force values in different target materials using the following semi empirical relation:

$$S_e = \frac{S_{High} S_{Low}}{S_{High} + S_{Low}} \tag{3}$$

In which $S_{Low}$ and $S_{High}$ are a low energy and high energy stopping power (see more details in Ref. [24]).

## Monte Carlo simulations

### Interatomic potential

The SRIM/TRIM Monte Carlo code developed by J.P. Biersack, J.F. Ziegler, U.Littmark and others [27], simulates the interaction of energetic ions with random targets using the binary collision approximation. It uses the universal potential or Ziegler-Biersack-Littmark (ZBL) potential to describe the ion-target collision, is given by [23]:

$$V_{ZBL}(r) = \frac{Z_1 Z_2 e^2}{4\pi\varepsilon_0 r} \phi\left(\frac{r}{a}\right) \tag{4}$$

In this expression, e is the electronic charge, $\varepsilon_0$ is the permittivity of free space, r is the interatomic distance, and a is an empirical screening length.

The universal screening function $\phi\left(\frac{r}{a}\right)$ is parameterized as a sum of exponentials expressed as [28]:

$$\phi\left(\frac{r}{a}\right) = \sum_{i=1}^{4} A_i e^{-B_i \frac{r}{a}} \tag{5}$$

Where $A_i$ and $B_i$ are fitting parameters. This function is determined by exact fitting of the calculated interatomic potentials of 522 randomly chosen pairs of atoms. The screening length depends on the atomic numbers and the Bohr radius by semi-empirical formula [23]:

$$a = \frac{0.8854 a_0}{Z_1^{0.23} + Z_2^{0.23}} \tag{6}$$

Where $a_0$ is the Bohr radius, it is equal 0.529 Å

**Table 1** Input parameters of target materials used in the SRIM simulation

| Target material | Mass density (g/cm$^3$) | Thickness ($\mu m$) | Surface binding energy (eV) | | | Lattice binding energy (eV) | | | Displacement energy (eV) | | |
|---|---|---|---|---|---|---|---|---|---|---|---|
| **W** | 19.35 | 7 | W:8.68 | | | W:3 | | | W:25 | | |
| **W-Cr-Ti** | 10.36 | 7 | W: 8.68 | Cr: 4.12 | Ti:4.89 | W: 3 | Cr: 3 | Ti:3 | W: 25 | Cr: 25 | Ti:25 |
| **W-Cr-Y** | 10.34 | 7 | W: 8.68 | Cr: 4.12 | Y:4.24 | W: 3 | Cr: 3 | Y:3 | W: 25 | Cr:25 | Y:25 |
| **W-Cr-Si** | 9.62 | 7 | W: 8.68 | Cr: 4.12 | Si:4.7 | W: 3 | Cr: 3 | Si:2 | W: 25 | Cr:25 | Si:15 |

## Calculation details

Monte Carlo simulations were performed by means of the SRIM/ TRIM code (version 2013). This code is based on theoretical formulations and semi-empirical models. It includes quick calculations that appear as tables of stopping powers, range and straggling distributions for any ion at any energy in the range ~ (1 eV- 2GeV/u) in any elemental target [29]. More elaborate calculations include targets with complex multi-layer configurations. The software SRIM-2013, as one of the most accepted simulation programs, is frequently used to calculate nuclear and electronic stopping power, and ion range in matter [22, 30]. Since the stopping power prediction from the SRIM code is based on fits experimental data, it usually provides reasonable predictions [31]. The core of SRIM is a program Transport of Ions in Matter (TRIM). In this work, we have used these two programs. SRIM was used to perform MC simulations of the stopping power of $H^+$ and $He^+$ ions in pure tungsten (W) and advanced smart tungsten-based alloys (W-Cr-Si, W-Cr-Ti, W-Cr-Y), with energies varied from 0 to 10 keV. The chosen nuclear and electronic stopping power unit is $10^{-15}$ eV.cm$^2$. In TRIM set-up, type of damage calculation, type of incident ion, ion energy, ion incident angle, the total number of ions, and target composition (Thickness, Mass density, surface binding energy, lattice binding energy, and displacement energy) should be defined. While TRIM was used to perform MC simulations for the total number of vacancies per (Å-Ion), the total number of displacements per (Å-Ion), the total number of replacement collisions per (Å-Ion), and total target damage. These damage events created in pure W and W-alloys were calculated using the "Detailed Calculation with full Damage Cascades" option. Indeed, all ions bombard the surface under normal incidence. The total number of each type of ion impacting on each target was $10^5$ used in the simulation run in order to obtain better statistical values and to avoid higher fluctuations. Typically, the mass density of W, W-Cr-Si, W-Cr-Ti, and W-Cr-Y targets were 19.35, 9.62, 10.36 and 10.34 g/cm$^3$, respectively, while their thickness was 7 $\mu m$ [32]. Additionally, the TRIM code uses three key calculation parameters for the target material. These are the bulk binding energy $E_b$, displacement energy $E_d$ and surface binding energy $E_s$. These energy parameters of each atom were determined by default values supplied by the program. Hence, the TRIM calculations reveal bulk binding energies of 3 eV for W, Cr, Ti, Y and 2 eV for Si, while displacement energies of 25 eV for W, Cr, Ti, Y and 15 eV for Si. The surface binding energies assumed for the calculations were 8.68 eV for W, 4.12 eV for Cr, 4.7 eV for Si, 4.89 eV for Ti, and 4.24 eV for Y. All the parameters mentioned above.

describing the target material, are summarized in Table 1.

## Simulation results and discussion

In this section, we provide the numerical simulation results that have been obtained using SRIM code, reliable simple predictive graphics have been drawn which permit the estimation of six physical events that may occur during an ion bombardment process. The six physical events are as follows: nuclear stopping power, electronic stopping power, total number of vacancies per (Å-Ion), total number of displacements per (Å-Ion), total number of per replacement collisions (Å-Ion), and total target damage. We will study these processes under the influence of incident energy of $H^+$ and $He^+$ ion bombardment on plasma-facing materials, as mentioned above. This research will aid us in assessing the damage produced by energetic ions in order to select the best material, ultimately enhancing reactor performance.

## Nuclear stopping power

When energetic ions pass through the target surface, they cause a sequence of screened Coulomb collisions in which the ion's energy is split into two stopping parameters: nuclear stopping and electronic stopping. Nuclear stopping power ($S_n$) is the energy lost by a moving ion projectile per unit length traveled in the target nuclei, due to elastic collisions. This type of collision involves wide discrete energy losses and major angular deflection of the trajectory of the ion. It is already known that the $S_n$ is a linear function of the elastic sputtering yield [33]. Hence, it generates lattice disorder by displacing atoms from their lattice locations [34].

Figure 1 depicts the nuclear stopping power as a function of the incidence energy of the two (a) $H^+$ and (b) $He^+$ ions bombardment for four thin layers: W, W-Cr-Si, W-Cr-Ti, and W-Cr-Y. The incidence angle is defined from the

normal surface. From this figure, one can observe that the $S_n$ curve as a function of incidence energy increases at first, reaches a maximum, and then decreases as incidence energy increases. As a result, all of the curves show the same behavior of variation according to the incidence angle. From our findings, it turns out that the W-Cr-Si thin layer has the highest nuclear stopping power for two ions and is followed by W-Cr-Ti, W-Cr-Y, and W in descending order. However, there is competition between these plasma-facing materials in the range 4000 to 10,000 eV for $H^+$ ions and in the range 9000 to 10,000 eV for $He^+$ ions. Concerning $H^+$ ions, we can see that the W-Cr-Si, W-Cr-Ti, W-Cr-Y, and W have the maximum nuclear stopping power of 0.4084, 0.394, 0.3788, 0.3263 eV/ ($10^{15}$ atoms/cm$^2$) at 800, 1000, 1200, 2750 eV, respectively. In the case of the $He^+$ ions, the maximal $S_n$ of these plasma-facing materials in the same order is 2.898, 2.839, 2.762, and 2.436 eV/ ($10^{15}$ atoms/cm$^2$) at 1700, 2250, 2750, and 6000 eV, respectively. Consequently, the nuclear stopping power increases with increasing the mass number of the ion. The mass number of $H^+$ and that of $He^+$ are 1.008u and 4.003u, respectively. Indeed, under the influence of ion energy, the lower value of $S_n$ is causing fewer defects in a protective layer. Thus, we can conclude that the pure W is better than the W ternary alloys in DEMO because the higher value of $S_n$ causes atomic displacements that can lead to disorder or defect creation such as vacancies, interstitials, and combination/agglomeration in all types of targets.

## Electronic stopping power

When the incoming ion interacts due to the inelastic collisions with an electron in the target while passing through it, one talks about electronic stopping power ($S_e$). The term 'inelastic' refers to the possibility that the collision will excite both the electrons of the target atoms and the incident ions' electron clouds [34]. Figure 2 illustrates the electronic stopping power versus incidence energy of $H^+$ and $He^+$ ions in four candidate plasma-facing materials at a normal incident. We remark two distinct regimes in Fig. 2a, b. Initially ($E \leq 100$ eV), the $S_e$ assumes a slow increase. Then, for larger energy ($E > 100$ eV), the $S_e$ appears to have a steep increase. As demonstrated in Fig. 2a, in the entire range of incidence energy, there is competition between values of the $S_e$ of $H^+$ ion in W, W-Cr-Si, W-Cr-Ti, and all thin layers in the range 0- 100 eV. Furthermore, one can see that the $S_e$ of the $H^+$ in W, W-Cr-Si, and W-Cr-Ti is equal and is lower than that in the W-Cr-Y in the region of $10^2$-$10^4$ eV. In Fig. 2b, the $S_e$ values of $He^+$ in all of the materials are nearly comparable, although, in the $10^3$-$10^4$ eV region, the $S_e$ in pure W is successively higher than that in W-Cr-Y, W-Cr-Ti, and W-Cr-Si. It is worth noting that the hardness and electrical conductivity enhance when electronic stopping power increases and nuclear stopping power reduces [35]. Seeing as W-Cr-Y has the greatest $S_e$ values of $H^+$ as compared to all layers at high incident energy, but it has the greatest $S_n$ values of $H^+$ as compared to W (referring to Fig. 1(a) and 2(a)). As a result, there is no improvement in surface hardness and electrical conductivity in W-Cr-Y layer. In the matter of $He^+$, it is noted that the W has these two qualities because its $S_e$ values are maximum at high energy and its $S_n$ values are minimum compared to ternary alloys.

## Collision events

While studying collision events, it is worth noting that [35],

Displacements = Vacancies + Replacement Collisions (7).

The sum of vacancies and replacement collisions corresponds to the displacements. These three main factors provide information on damage events created in plasma-facing materials in DEMO.

## Target vacancies

The number of vacancies formed in a material by ion bombardment is an important physical measure for describing material removal efficiency. The total vacancies refer to holes left behind when a recoil atom moves from its original site. Indeed, when a material has defects, it is usually less resistant to sputtering; the existence of defects impacts the material's electrical and mechanical properties. Figure 3 shows the plot of the total number of vacancies per length (Å) per ion bombardment (a) $H^+$ and (b) $He^+$ generated in four layers versus the incident energy. We notice here that the total number of vacancies per (Å-Ion) increases by increasing the incident energy in the range of 0 to 10 keV. In addition, the total number of vacancies per (Å-Ion) due to $He^+$ ions is higher than that due to $H^+$ ions. Under the influence of ion energy for $H^+$, we can see that the W-Cr-Si layer has the highest total number of vacancies and is followed by W-Cr-Ti, W-Cr-Y, and W in descending order, as illustrated in Fig. 3a.

In the case of the $He^+$ ions, the gap between two W-Cr-Ti and W-Cr-Y layers is narrower, given in Fig. 3b. In general, the amount of W vacancies formed per (Å-Ion) in direct collisions is found to be lower than that of W-Cr-Si, W-Cr-Ti, and W-Cr-Y. Hence, we can conclude that the pure W layer reduces the total number of vacancies per (Å-Ion) generated by ion sputtering by comparing it with ternary alloys layers.

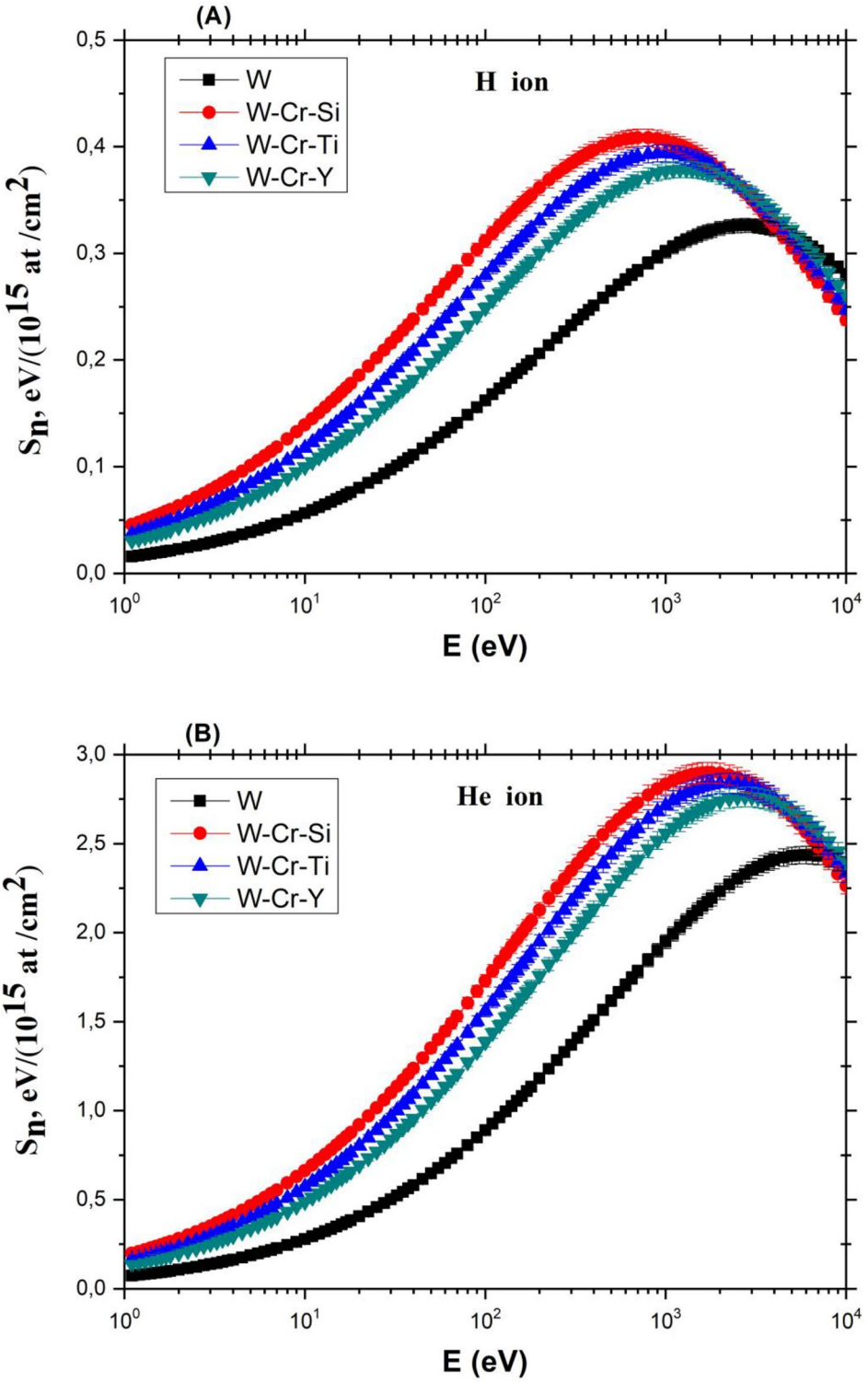


**Fig. 1** Nuclear stopping power ($S_n$) for collisions of (a) $H^+$ and (b) $He^+$ ions with targets made of W-Cr-Y, W-Cr-Ti, and W-Cr-Si versus incident ion energy using the SRIM-2013 program. The results obtained are compared with the pure W target

## Replacement collisions

If a traveling atom collides with a stationary target atom and transfers more energy to it than it has, and the initial atom has insufficient energy to continue moving, and it is the same element as the atom it impacted, it simply replaces that atom

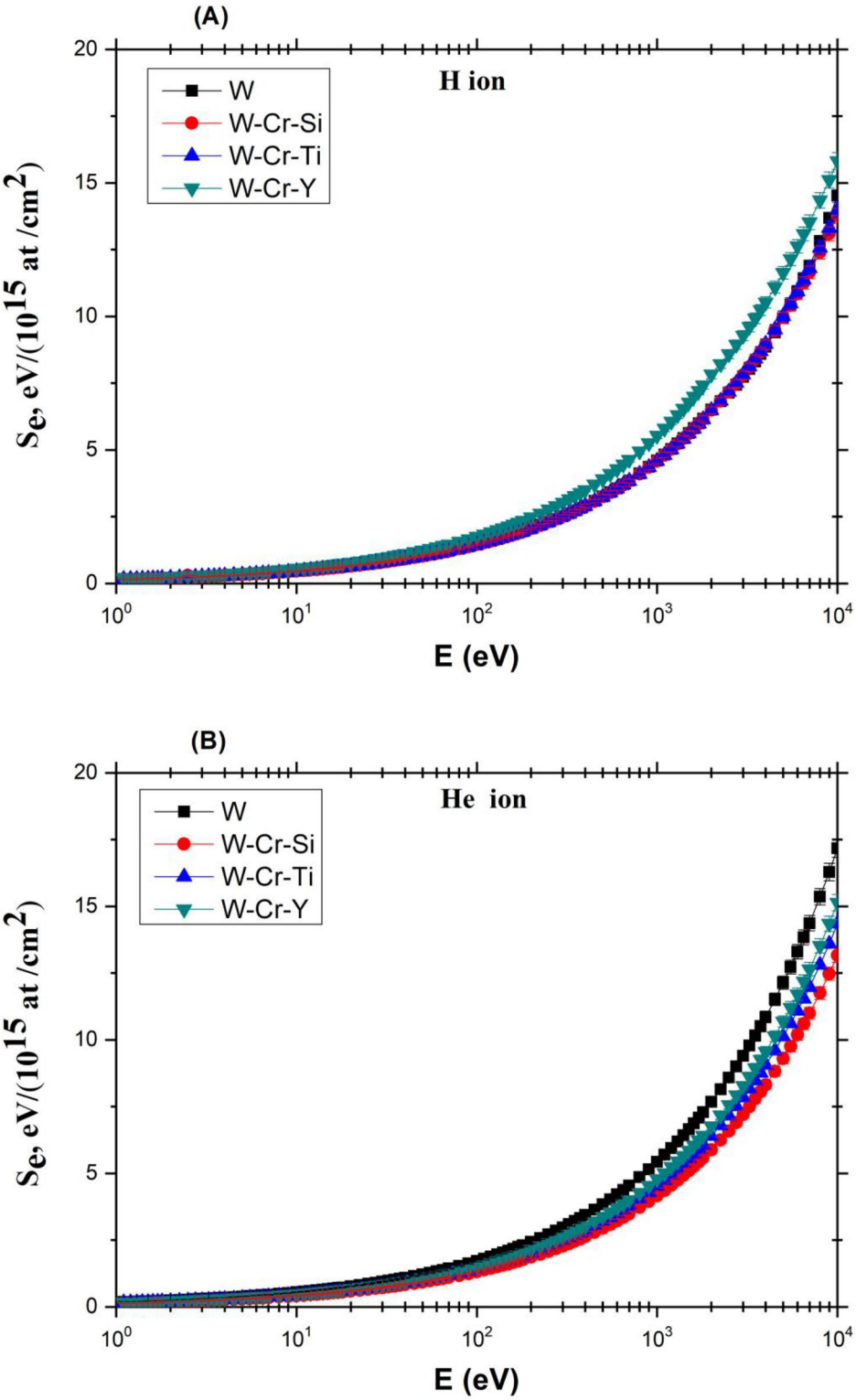


**Fig. 2** Electronic stopping power ($S_e$) for collisions of (a) $H^+$ and (b) $He^+$ ions with smart tungsten alloys depending on the incident ion energy using the SRIM-2013 program. The results obtained are compared with the pure W target

in the target, leaving no vacancy. These are called replacement collisions [36]. It refers to the difference in number of total displacements and total vacancies. Figure 4 represents the effect of the incident ion energy on the total number of

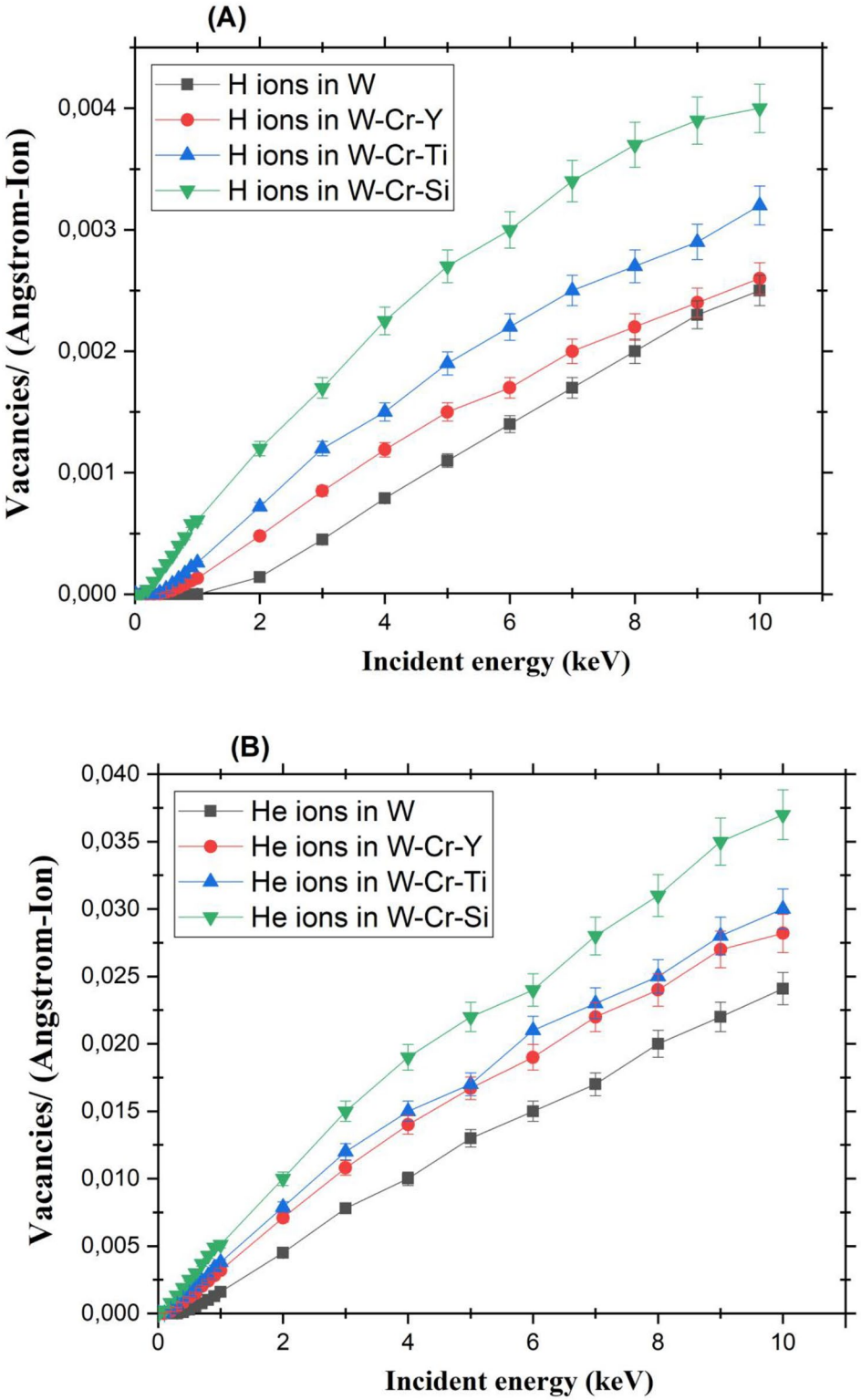


**Fig. 3** Total vacancies per length (Å) per ion created in W and its smart alloys layers by (a) $H^+$ and (b) $He^+$ ion bombardment as a function of the incident ion energy using the SRIM-2013 program

replacement collisions per (Å-$H^+$ ion) and per (Å- $He^+$ ion) in four thin films at normal incidence. Over the whole range of incident energy, the total number of replacement collisions per (Å-Ion) bombardment increases with the increase

of incident energy. Figure 4a, b present that the slope of the total number of replacement collision per (Å-$He^+$ ion) is more than that per (Å- $H^+$ ion). In Fig. 4a, we can decompose the curve of the total number of replacements into two parts. The first part where the incident energy varies from 0 to 3 keV, we find that the numbers of replacement in W-Cr-Si are higher. The second part where the incident energy exceeds 3 keV, it turns out that the total number of replacement collision per Å per $H^+$ ion bombardment in pure W layer is higher than that in ternary alloys (W-Cr-Si, W-Cr-Ti, and W-Cr-Y). On the other hand, we see in Fig. 4b that at low incident energy (around 0 to 1 keV), there is competition between all layers. However, when the incident energy overpasses 1 keV, it is clear that the total number of replacement collisions per (Å-$He^+$ ion) in pure W is greater than in the ternary alloys. As a result, pure W is regarded as a good protective layer to substitute ternary alloys since it exhibits a superior number of replacement collisions, resulting in higher resistance to vacancies than ternary alloys (referring to Fig. 3).

## Target displacement

The total number of displacements refers to the number of atoms knocked off their target lattice site by collision processes if their kinetic energy is above the displacement threshold energy ($E > E_d$). The displacement of target atoms has a number of consequences, including the sputtering yield of surface atoms, generation and migration of point defect, and formation of surface layers with different properties relative to the bulk target [34]. Figure 5 shows the total displacement per Å per ion bombardment (a) $H^+$ and (b) $He^+$ created in four ternary alloys thin layers as a function of the ion impact energy. It is seen here, that the total displacement per (Å-Ion) values increase with an increase in both ion energy and ion mass number, as illustrated in Fig. 5a, b. From this figure, it is obvious that the highest total number of displacements per (Å- Ion) is found in the W-Cr-Si layer and the lowest one is found in the pure W layer. Meanwhile, we note that under 9–10 keV $H^+$ ion bombardment, both W and W-Cr-Y layers are equivalent. It can be concluded that ion bombardment produces fewer lattice disorders in the pure W thin layer by comparing it with the ternary alloys' thin layers.

## Total target damage

Figure 6 represents total target damage (keV/ion) as a function of incident energy of two $H^+$ and $He^+$ ions at normal incidence for (a) W, (b) W-Cr-Si, (c) W-Cr-Ti, and (d) W-Cr-Y. As can be seen from Fig. 6 (a-d), the total target damage increases monotonically with the incident energy of the $He^+$ ion. In addition, the total target damage values produced by $He^+$ ions are greater than those by $H^+$ ions. Hence, the higher mass number of incident ion gives the higher production of total target damage. On the other hand, about $H^+$ ions, we observe at the beginning the absence of total target damage of W, W-Cr-Y, and W-Cr-Si in the range of 0–5 keV, 0–3 keV, and 0–2 keV, respectively. After these intervals, the total target damage remains constant at the value of 0.01 keV/ion, except for W-Cr-Si which goes from this value to 0.02 keV/ion at 10 keV. One can also see that total target damage for W-Cr-Ti under $H^+$ ion bombardment increases as the incident energy changes from E = 0 keV to E = 1 keV, but it remains constant at the same value (0.01 keV/ion) when the incident energy changes from 1 to 10 keV.

It is interesting to note that the W-Cr-Si layer has the greatest total target damage values while the pure W layer has the lowest. Because the W-Cr-Si layer has the lowest mass density (9.62 g/cm$^3$) and pure W has the highest ones (19.35 g/cm$^3$). Furthermore, it is discovered that two competing layers exist between them: W-Cr-Ti and W-Cr-Y, which have about the same mass density (10.36 and 10.34 g/cm$^3$, respectively). As a result, it is widely considered that as mass density decreases, the total target damage increases, particularly at high energy levels. It can be concluded that the pure W layer minimizes total damage caused by the $He^+$ ion by comparing it with the ternary alloys' layers.

Several independent measurements were taken for each incident energy, and the error bar shows the amount of standard deviation for all valid data at that energy. The data point is the average (arithmetic mean) of such data.

## Conclusions

We have developed a parameter set suitable for characterizing the collision between four leading candidate plasma-facing materials (W, W-Cr-Si, W-Cr-Ti, and W-Cr-Y) and ion bombardments with $H^+$ and $He^+$ ions in a DEMO fusion power plant. By carrying out the Monte Carlo simulations code SRIM, we have calculated the six physical events as a function of ion energies at normal incidence. These include nuclear stopping power, electronic stopping power, the total number of vacancies per (Å-Ion), the total number of displacements per (Å-Ion), the total number of replacement collisions per (Å-Ion), and the total damage in four candidate plasma-facing materials. The obtained results clearly demonstrate that these physical processes are dependent on the ion energy, the masses of the ion and the target's atoms.

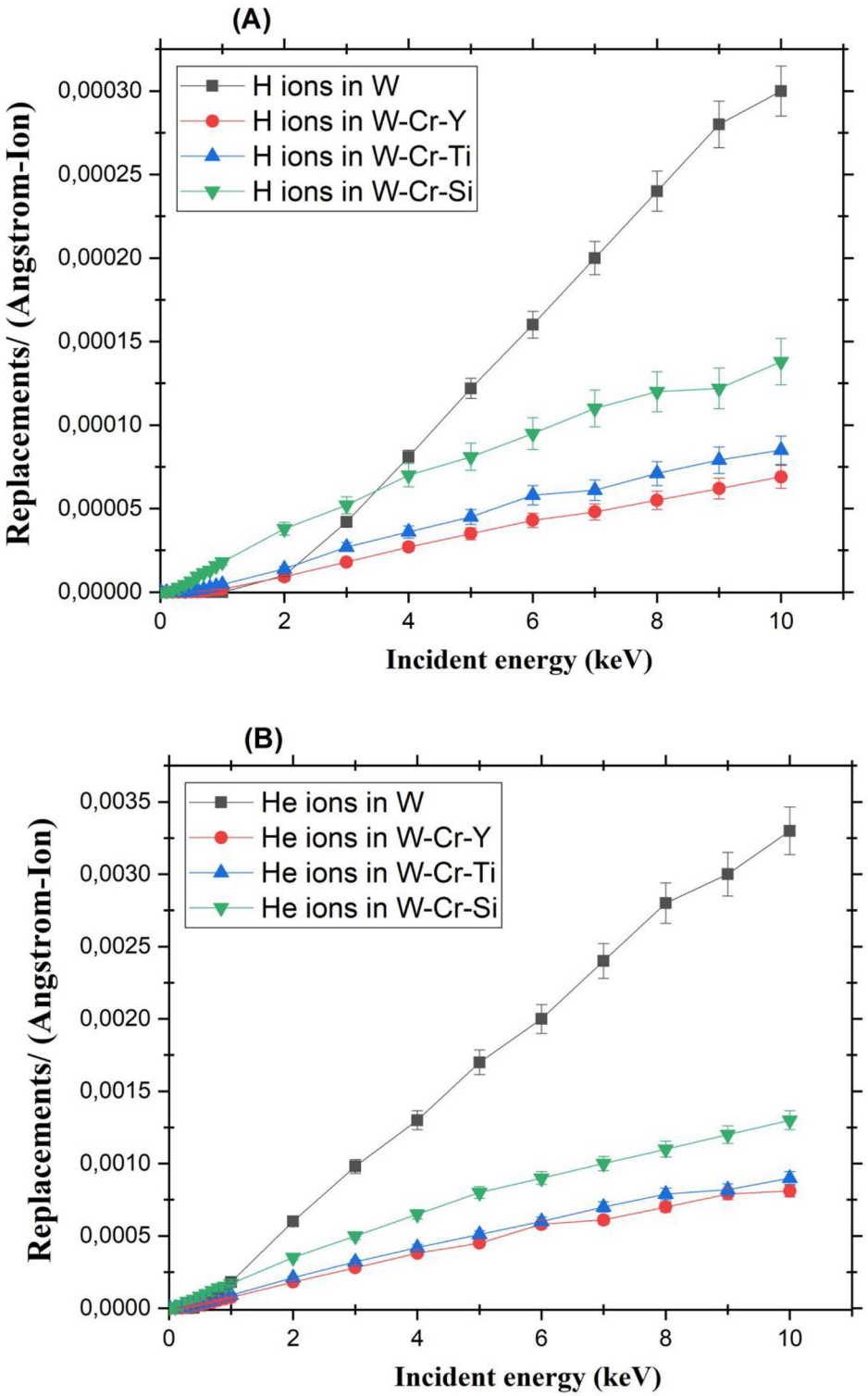


**Fig. 4** Total replacements per length (Å) per ion in W and its smart alloys layers by (a) $H^+$ and (b) $He^+$ ion bombardment as a function of the incident ion energy using the SRIM-2013 program

We have found that the W-Cr-Si thin layer is giving the weakest performance compared to all other thin layers because it has the highest $S_n$ for two ions and is followed by W-Cr-Ti, W-Cr-Y, and W in descending order. However, there is competition between these layers in the range of 4 to 10 keV for $H^+$ ions and in the range of 9 to 10 keV for $He^+$

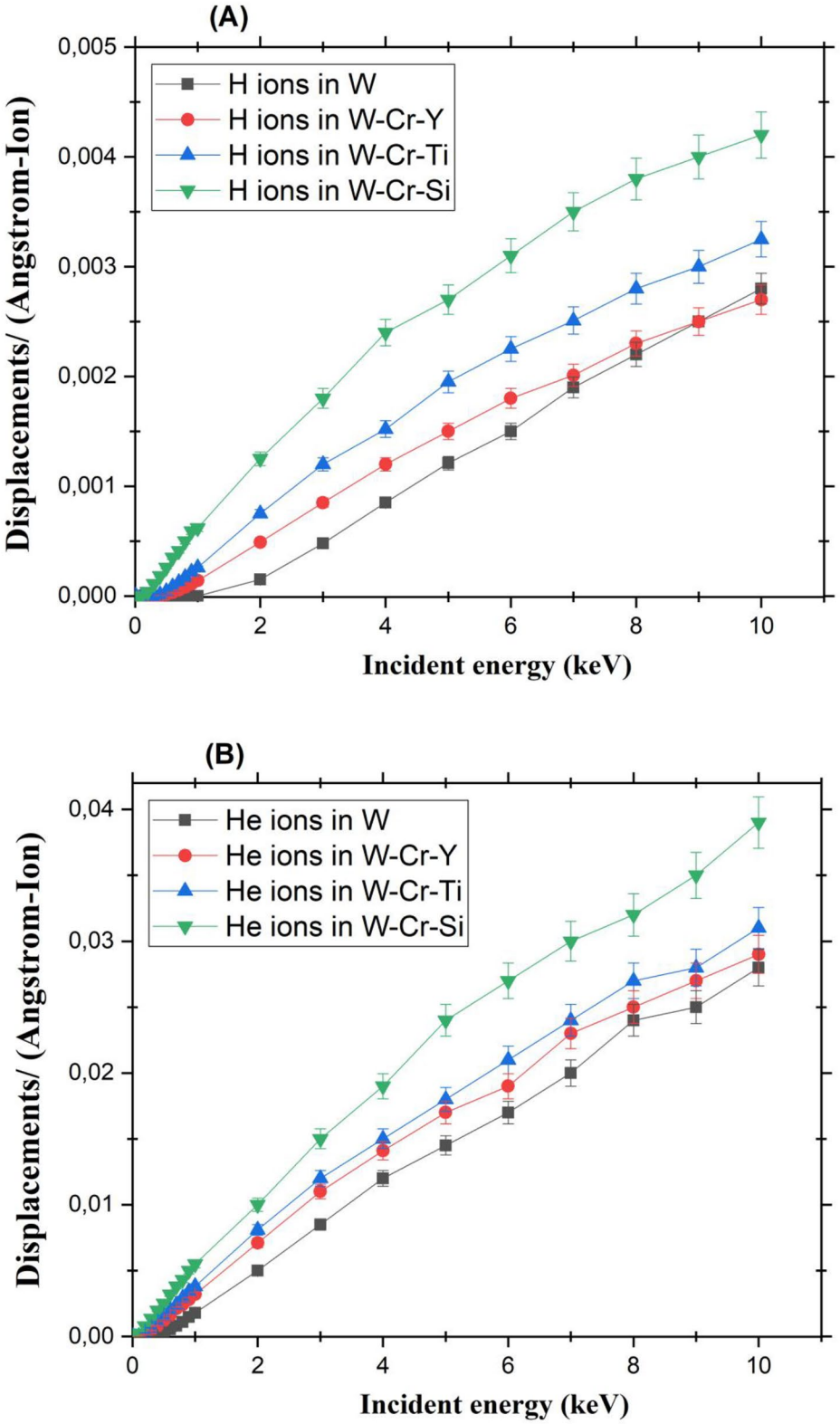


**Fig. 5** Total displacements per length (Å) per ion in W and its smart alloys layers by (a) $H^+$ and (b) $He^+$ ion bombardment as a function of the incident ion energy using the SRIM-2013 program

ions. In addition, it has a higher total number of vacancies per (Å- $H^+$ Ion or Å- $He^+$ Ion), a higher total number of

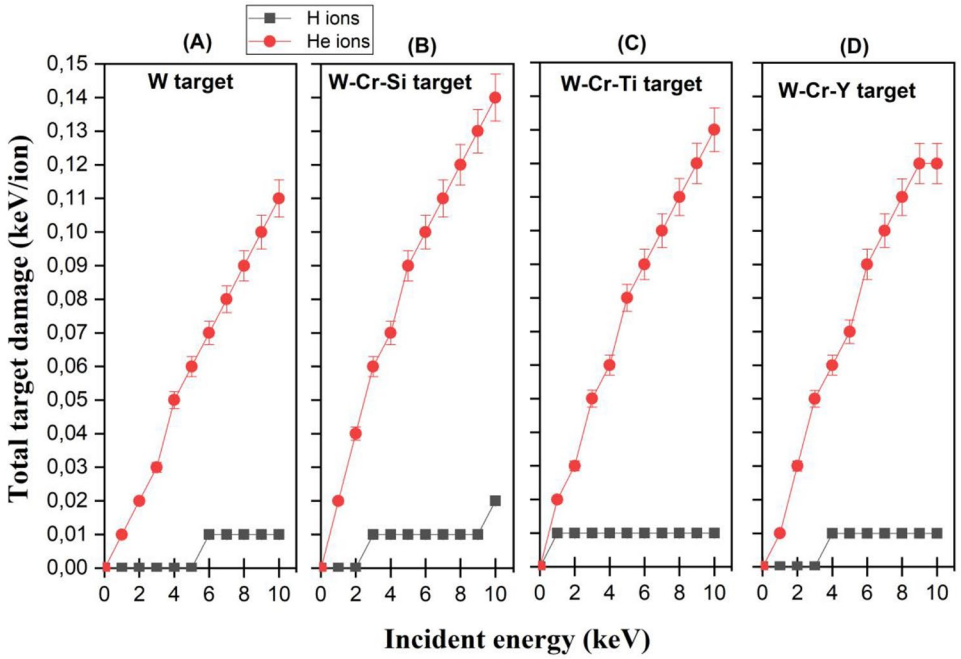


**Fig. 6** Total target damage as a function of incident energy of two $H^+$ and $He^+$ ions for (a) W, (b) W-Cr-Si, (c) W-Cr-Ti, and (d) W-Cr-Y using the SRIM-2013 program

displacements per (Å- $H^+$ or $He^+$ Ion) and higher total damage, despite having a higher total number of replacements per (Å- $H^+$ Ion) at incident energies between 0 and 3 keV.

Despite the fact that W-based smart alloys can greatly reduce the oxidation rate compared to pure W. In this study, we found that the pure W thin layer outperforms all smart alloy protective layers in terms of the total number of vacancies per (Å- $H^+$ Ion or Å- $He^+$ Ion), the total number of replacements per (Å-$He^+$ Ion), the total number of displacements per (Å- $H^+$ Ion or Å- $He^+$ Ion), and total target damage. The W thin layer has the highest total number of replacements per (Å-$He^+$ Ion), the lowest total number of vacancies per (Å- $H^+$ Ion or Å- $He^+$ Ion), and the lowest total number of displacements per (Å- $He^+$ Ion), as well as the least total damage over the entire range of incidence energies (0–10 keV). It is worth noting that the hardness and electrical conductivity enhance when electronic stopping power ($S_e$) increases and nuclear stopping power reduces. In the matter of $He^+$, it is noted that the W has these two qualities because its $S_e$ values are maximum at high energy and its $S_n$ values are minimum compared to ternary alloys. In view of all results, W is widely regarded as the most promising armor material for future nuclear fusion power plants. It is resilient against vacancies, atomic displacement, total damage, and nuclear energy loss.

**Acknowledgements** The authors declare that they have no known competing financial interests or personal relationships that could have appear to influence the work reported in this paper.

## References

1. Minucci S, Panella S, Ciattaglia S, Falvo MC, Lampasi A (2020) Electrical loads and power systems for the DEMO nuclear fusion project. Energies 13(9):2269
2. Federici G, Boccaccini L, Cismondi F, Gasparotto M, Poitevin Y, Ricapito I (2019) An overview of the EU breeding blanket design strategy as an integral part of the DEMO design effort. J Fus Eng Design 141:30–42
3. Day Chr, Butler B, Giegerich T, Lang PT, Lawless R, Meszaros B (2016) Consequences of the technology survey and gap analysis on the EU DEMO R&D programme in tritium, matter injection and vaccum. J Fus Eng Design 109:299–308
4. Pitts RA, Carpentier S, Escourbiac F, Hirai T et al (2011) Physics basis and design of the ITER plasma-facing components. J Nucl Mater 415(1):S957–S964
5. Troev T, Popov E, Staikov P, Nankov N, Yoshiie T (2009) Positron simulations of defects in tungsten containing hydrogen and helium. J Nucl Instrum Methods Phys B 267(3):535–541
6. Pospieszczyk A, Brezinsek S, Mertens Ph, Sergienko G (2002) The role of hydrogen atoms and molecules in the plasma boundary. Contrib Plasma Phys 42(6–7):663–667
7. Fu T, Cui K, Zhang Y, Wang J, Shen F, Yu L, Qie J, Zhang X (2021) Oxidation protection of tungsten alloys for nuclear fusion applications: A comprehensive review. J Alloys Compd 884:161057
8. Litnovsky A, Schmitz J, Klein F, Lannoye KD et al (2020) Smart tungsten-based alloys for a first wall of demo. J Fus Eng Design 159:111742
9. Bachurina D, Tan XY, Klein F, Suchkov A, Litnovsky A et al (2021) Self-passivating smart tungsten alloys for DEMO: a progress in joining and upscale for a first wall mockup. Tungsten 3(1):101–115
10. Litnovsky A, Klein F, Tan X, Ertmer J et al (2021) Advanced self-passivating alloys for an application under extreme conditions. Metals 11(8):1255

11. Yi G, Liu W, Ye C, Xue L, Yan Y (2021) A self-passivating W-Si-Y alloy: Microstructure and oxidation resistance behavior at high temperatures. Corros Sci 192:109820
12. Koch F, Bolt H (2007) Self passivating W-based alloys as plasma facing material for nuclear fusion. Physica Scripta 2007 (T128):100
13. Koch F, Kôppl S, Bolt H (2009) Self passivating W-based alloys as plasma facing material. J Nucl Mater 386:572–574
14. Liu DG, Zheng L, Luo LM, Zan X, Song JP, Xu Q, Zhu XY, Wu YC (2018) An overview of oxidation-resistant tungsten alloys for nuclear fusion. J Alloys Compd 765:299–312
15. Hou QQ, Huang K, Luo LM, Tan XY, Zan X, Xu Q, Zhu XY, W YC (2019) Microstructure and its high temperature oxidation behavior of W-Cr alloys prepared by spark plasma sintering. Materialia 6:100332
16. Zhao Z, Li Y, Zhang C, Pan G, Tang P, Zeng Z (2017) Effect of grain size on the behavior of hydrogen/helium retention in tungsten: a cluster dynamics modeling. J Nucl fus 57(8):086020
17. Brooks JN, Allain JP, Doerner RP, Hassanein A, Nygren R, Rognlien TD, Whyte DG (2009) Plasma-surface interaction issues of an all-metal ITER. J Nucl fus 49(3):035007
18. Correa AA (2018) Calculating electronic stopping power in materials from first principles. Comput Mater Sci 150:291–303
19. Andersen HH, Brunelle A, Della-Negra S, Depauw J, Jacquet D, Beyec YL, Chaumont J, Bernas H (1998) Giant metal sputtering yields induced by 20-5000 keV/atom gold clusters. Phys Rev lett 80(24):5433
20. Meluzova DS, Babenko PY, Shergin AP, Nordlund K, Zinoviev AN (2019) Reflection of hydrogen and deuterium atoms from the beryllium, carbon, tungsten surfaces. J Nucl Instrum Methods Phys B 460:4–9
21. Zinov'ev AN, Babenko PY (2020) Nuclear stopping power of hydrogen and helium isotopes in beryllium, carbon, and tungsten. Tech Phys Lett 46(9):909–912
22. Weber WJ, Zhang Y (2019) Predicting damage production in monoatomic and multi-elemental targets using stopping and range of ions in matter code: Challenges and recommendations. Curr Opin Solid State Mater Sci 23(4):100757
23. Paul H (2013) Nuclear stopping power and its impact on the determination of electronic stopping. Power-AIP Conference Proceedings 1525(1):309–313
24. DIB A, Ammi H, Msimanga M, Mammeri S, Pineda-Vargas CA (2019) Energy loss and stopping force of heavy ions Cu,Si, Al and F through thin Nickel (Ni) foil at low MeV energies. J Nucl Instrum Methods Phys B 450:43–46
25. Duan G, Xing T, Li Y (2012) Preferential sputtering of Ar ion processing SiO2 mirror. AOMATT, the 6th International Symposium on advanced Optical Manufacturing and Testing Technologies 8416:585–592
26. Anderson HH, Ziegler JF (1977) Helium stopping powers and ranges in all elements
27. Saha U, Devan K, Ganesan S (2018) A study to compute integrated dpa for neutron and ion irradiation environments using SRIM-2013. J Nucl Mater 503:30–41
28. Ahn HS, Kim TE, Cho E, Ji M, Lee CK, Han S, Cho Y, Kim C (2008) Molecular dynamics study on low-energy sputtering properties of MgO surfaces. J Appl Phys 103(7):073518
29. The stopping and range of Ions in Matter [online]. www.srim.org
30. Yalçin C(2015) Thickness measurement using alpha spectroscopy and SRIM. J Physics: Conference Series. IOP Publishing 590(1): 012050
31. Zhang Y, Lian J, Zhu Z, Bennett WD, Saraf LV, Rausch JL, Hendricks CA, Ewing RC, Weber WJ (2009) Response of strontium titanate to ion and electron irradiation. J Nucl Mater 389(2):303–310
32. Litnovsky A, Wegener T, Klein F, Linsmeier C et al (2017) Advanced smart tungsten alloys for a future fusion power plant. Plasma Phys Controlled Fusion 59(6):064003
33. Rautray TR, Narayanan R, Kim KH (2011) Ion implantation of titanium based biomaterials. Prog Mater Sci 56(8):1137–1177
34. Ali SH, Saeed SR (2014) Theoretical calculation of different ion surface interaction parameters of Si target. J zankoy sulaimani-Part (JZS-A) 16(1):1
35. Giri K, Kandel B (2020) Study of damage profiles and energy calculation of arsenic ions during ion implantation on germanium. BIBECHANA 17:96–103
36. Mahady K, Tan S, Greenzweig Y, Livengood R, Raveh A, Rack P (2016) Monte Carlo simulations of nanoscale $Ne^+$ ion beam sputtering: investigating the influence of surface effects, interstitial formation, and the nanostructural evolution. Nanotechnology 28(4):045305